Experimental Investigation: Stability Criteria of an Uncambered Airfoil in Ground Effect

S.C. Rhodes[a] and A.T. Sayers[b]

Received 29 September 2008, in revised form 17 June 2009 and accepted 21 July 2009

Experiments have been conducted to determine the effect of flat ground proximity on the aerodynamic characteristics of a slender un-cambered Department of Hydro-Mechanics of the Marine Technical University (DHMTU) rectangular wing of aspect ratio 3. The experiments were performed to provide data for an ongoing experimental and computational fluid dynamics (CFD) study examining the effects of non-flat ground on the performance of wings in ground effect. The wing was tested in an open jet wind tunnel test section fitted with a flat moving ground plane. Experimental measurements were carried out at a flow Reynolds number of 2.2×10^5 ***for relative ground clearances of*** $0.06 < h_0 < 1.8$***, and angles of attack between –9 and 37°. Data is presented for lift, drag, pitching moment, aerodynamic centre in pitch (ACP), aerodynamic centre in height (ACH) and static stability margin (SSM) versus angle of attack and ground clearance. The data shows that at relative ground clearances*** $h_0 < 0.5$***, the wing experiences a rapid deterioration of the SSM for typical flight cruise angles. This effect is attributed to a loss in lift as the ground is approached. The ACH was found to be predominantly behind the ACP. The SSM was, thus, predominantly negative at all ground clearances, implying that the wing was unstable in ground effect.***

Nomenclature

Roman

AR	aspect ratio (b^2/S)
b	wing span
c	wing chord
$\bar{c}$	mean aerodynamic chord (mac)
C_D	drag coefficient
C_L	lift coefficient
$C_{L.max}$	maximum lift coefficient
C_M	moment coefficient
D	drag
h_0	relative ground clearance ($= h / \bar{c}$)
H	ground clearance, measured between the belt and the trailing edge of the wing
L	lift
M	pitching moment (about ¼ mac)
q	dynamic pressure ($=1/2\rho V^2$)
R_e	Reynolds number ($= \rho V \bar{c} / \mu$)
S	wing area
V	free air stream velocity
X_α	location of aerodynamic centre in pitch (*ACP*)
X_h	location of aerodynamic centre in height (*ACH*)

Greek

α	angle of attack
α_{L0}	angle of attack at zero lift
α_{stall}	stall angle
μ	free air stream dynamic viscosity
ρ	free air stream density

1. Introduction

The phenomenon today known as ground effect was observed very early in the birth of aviation. Pilots would note their aircraft tended to "float" in the air when close to the ground. The benefits of operating an aircraft in ground effect are generally recognised by an increase in lift and decrease in drag, translating to an increase in load carrying capacity and range.

As early as 1921, Wieselsberger[1] theoretically and experimentally analysed the effect of the ground on wings. In 1935 Kaario designed one of the first craft engineered to take advantage of ground proximity effects[2]. Throughout the 'cold war' era, Rostislav Alekseev and Alexander Lippisch made significant contributions to the field. In 1966, Alekseev designed the largest wing in ground effect (WIG) craft flown to date. Known as the KM, it was over 500 feet long and weighed 550 tons[3].

However, the benefits of operating in ground effect are not without complication. To date, only conventional wing-tail configurations demonstrate sufficient levels of pitch stability for sustained operation in ground effect. Furthermore, to achieve pitch stability, horizontal stabilizers are typically 20 to 80 % larger than conventional aircraft with the same moment arm[4]. Kumar[5, 6], Irodov[7], Zhukov[8], and Staufenbiel and Schlichting[9] all addressed the issue of pitch stability in ground effect; determining that the relative position of the aerodynamic centre in height and pitch influenced the nature of the pitch stability.

Numerous studies have been conducted analysing the influence of the ground on wing performance[10, 11]. However, few papers discuss wing performance with particular attention paid to the two aerodynamic centres. Hence, the inherent stability near the ground is largely overlooked. Rozhdestvensky[4] presents a synopsis of research examining the influence of wing profile and planform on the positioning of the two aerodynamic centres. Gadetski[12], one of the first researchers to identify a trailing edge flap as a means of improving stability, found the upward deflection of the trailing edge improved pitch stability in ground effect. Staufenbiel and Kleineidam[13]

a, b Department of Mechanical Engineering
University of Cape Town, Private Bag X3
Rondebosch, 7701, South Africa
b Member SAIMechE
E-mail: Anthony.Sayers@uct.ac.za

identified a wing with an *S*-shaped mean line, as well as the sweeping of the wing tips, as further enhancing pitch stability.

However, the majority of such studies are conducted as analytical and numerical investigations. Some research is validated through wind tunnel experiments, but the generation of such data is greatly complicated by the presence of the simulated ground. Furthermore, correctly simulating the ground in a tunnel requires specialised equipment. These factors are a major cause for the relatively low number of wind tunnel experiments in ground effect.

This study serves to contribute further experimental data to the existing body of knowledge specific to aerodynamic ground effect. The study also forms part of an ongoing CFD study concerning wing-in-ground effect.

Presented in the following sections are the general equations required for the analysis of longitudinal static stability; the experimental apparatus to determine the lift, drag and moments on the wing; the test procedure; and a matrix of lift, drag, and pitching moment data presented as a function of angle of attack (AoA) and ground clearance for a wing in and out of ground effect.

2. Static Longitudinal Stability in Ground Effect

Aircraft operating in close proximity to the ground can experience significant changes in the aerodynamic forces acting upon them. For positive angles of attack, below the stalled condition, the influence of the ground, in general, produces an increase in the lift-to-drag (L/D) ratio. This arises as a result of the restriction in the development of the wing-tip vortices, and, an increase in pressure between the wing and the ground[3]. These changes usually only become significant for ground clearances less than the length of the mean aerodynamic chord (mac). For this reason, the ground clearance is usually non-dimensionalised relative to the mac of the primary lifting surface. This description of the relative ground clearance is denoted as $h_0 = h/\bar{c}$ where the ground clearance, *h* is measured from the trailing edge (TE) of the wing, and $\bar{c}$ is the mean aerodynamic chord of the wing.

All lifting surfaces in close proximity to the ground are susceptible to pitch instability as a result of the changing aerodynamic forces. The static longitudinal stability of a wing in ground effect can be evaluated by analysis of the derivatives of the lift coefficient, C_L and the moment coefficient, C_M with respect to the angle of attack, α and the relative ground clearance h_0 respectively. The principle variables involved (figure 1) are the lift, *L*, drag, *D*, and pitching moment, *M*. They act on a wing of chord, *c*, at an angle of attack α, and at a height, *h*, above a flat ground plane. The reference point for all moments is the ¼ mac unless otherwise stated. The ground plane moves with a velocity *V* in a free stream of velocity *V*, density ρ and dynamic viscosity μ.

The derivatives of C_L and C_M are written in the following way for convenience;

$$C_{L\alpha} = \frac{\partial C_L}{\partial \alpha} \tag{1}$$

$$C_{M\alpha} = \frac{\partial C_M}{\partial \alpha} \tag{2}$$

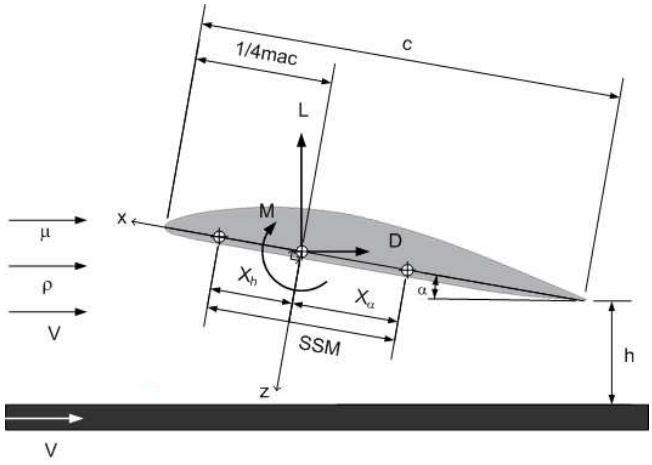

Figure 1: Wing in ground effect

$$C_{Lh} = \frac{\partial C_L}{\partial h_0} \tag{3}$$

$$C_{Mh} = \frac{\partial C_M}{\partial h_0} \tag{4}$$

The static longitudinal stability of a wing in ground effect depends upon the location of the aerodynamic centres in height and pitch. The position of the aerodynamic centre in pitch (ACP) is the point where C_M remains constant with changing angle of attack, α. It is defined as[2]:

$$X_\alpha = \frac{C_{M\alpha}}{C_{L\alpha}} \tag{5}$$

The position of the aerodynamic centre in height (ACH) is the point where C_M remains constant with changing height, h_0. It is defined as[2]:

$$X_h = \frac{C_{Mh}}{C_{Lh}} \tag{6}$$

Equations 5 and 6 give the non-dimensional *x*-coordinates of the ACP and ACH, relative to the moment axis, as a function of α and h_0 respectively. It should be noted these equations are approximations of the true aerodynamic centres and can only be considered accurate for small angles of attack and configurations where the lift is significantly larger than the drag. For most cruising aircraft these assumptions are valid. Figure 1 also illustrates the orientation of the relevant body-fixed coordinate system and nominal positions for X_α and X_h relative to the moment axis. A ground-effect craft must be stable in both height and pitch. A disturbance in pitch angle or in height above the surface must be compensated for by a restoring moment or force respectively. Static pitch stability is associated with a negative slope of the C_M vs. α curve and is given by[2];

$$C_{M\alpha} < 0 \tag{7}$$

Static height stability is associated with a negative slope of the C_L vs. h_0 curve and this is represented by[2];

$$C_{Lh} < 0 \tag{8}$$

A further condition for static height stability is that X_h is located upstream of X_α. If the positive direction of the body-fixed x-axis is upstream, Irodov's[6] criterion for static height stability is given by[2];

$$X_h - X_\alpha > 0 \tag{9}$$

The distance between the aerodynamic centres is referred to as the Static Stability Margin, SSM = $X_h - X_\alpha$. Figure 1 illustrates a positive SSM.

3. Experimental Apparatus and Procedure

3.1 Wind tunnel

The experiments were conducted in a closed return wind tunnel with an open jet test-section (figure 2). The test section had an octagonal profile, with a maximum height and width of 580 mm and 876 mm respectively. The maximum airspeed achievable in the test section was 30 m/s. The static pressure gradient along the test section was approximately zero with a turbulence intensity of 0.4 %. The dynamic pressure was measured near the tunnel centreline using an inclined manometer. A 3-component force balance, positioned in the over-tunnel configuration, was used to measure the lift, drag and pitching moment to accuracies of 0.222 N, 0.0890 N and 0.0170 Nm respectively, while the height of the balance above the moving ground plane was adjustable to within an accuracy of 0.5 mm over a range of approximately 300 mm ($\approx 2\,\bar{c}$).

3.2 Moving ground plane

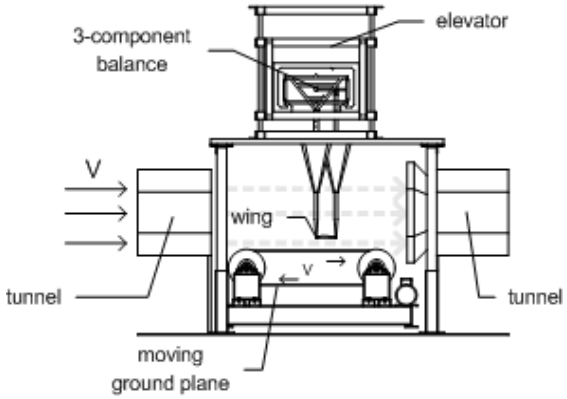

Figure 2: Wind tunnel test section

A rolling road type moving-belt was used to simulate the ground plane. The belt had a span of 890 mm and revolved around two steel cylinders one of which was driven by an electric motor. The cylinders had a diameter of 275 mm and an axle spacing of 1060 mm. No bevel or surface profiling was made across the cylinders; however, the surfaces were knurled to improve belt-cylinder contact.

The belt itself was formed from two-ply, reinforced polyvinyl chloride (PVC), with the ends hot welded to form a loop and to ensure smooth running over the cylinders at high speed.

3.3 Model wing

A DHMTU 10-40-2-10-2-60-21-5 rectangular airfoil with a span, b, of 465 mm and a chord, c, of 155 mm (aspect ratio, AR = 3) was tested. The relatively slender wing (figure 1) had a 10 % maximum thickness ratio (t/c) at a chordwise station from the leading edge, x/c = 40 %. The wing had a flat section on the lower surface from x/c = 10 % to x/c = 60 %. The flat section was parallel to the chord and 2 % below it. The nose radius parameter was 5. The coordinates of the wing were generated using a DHMTU profile generator[14] and are listed in table 1.

The wing was suspended from the 3-component balance by three vertical struts that were enclosed in streamlined shields to obviate drag on them from the free stream. The wing was attached to the struts through trunnion pins at points 115 mm in from the wing tips along the leading edge, and at the centre of the trailing edge, such that it was able to pivot about its leading edge trunnion pins while the rear strut could be adjusted vertically to change the angle of attack.

Station	x/c	y/c	Station	x/c	y/c
0	1	0	25	0	0
1	0.9961	-0.0006	26	0.0039	0.0071
2	0.9843	-0.0023	27	0.0157	0.0159
3	0.9649	-0.0048	28	0.0351	0.0262
4	0.9382	-0.0079	29	0.0618	0.0376
5	0.9045	-0.0112	30	0.0955	0.0498
6	0.8645	-0.0142	31	0.1355	0.0621
7	0.8187	-0.0167	32	0.1813	0.0739
8	0.7679	-0.0185	33	0.2321	0.0844
9	0.7129	-0.0196	34	0.2871	0.0929
10	0.6545	-0.0199	35	0.3455	0.0983
11	0.5937	-0.02	36	0.4063	0.1
12	0.5314	-0.02	37	0.4686	0.0978
13	0.4686	-0.02	38	0.5314	0.0924
14	0.4063	-0.02	39	0.5937	0.0844
15	0.3455	-0.02	40	0.6545	0.0743
16	0.2871	-0.02	41	0.7129	0.0632
17	0.2321	-0.02	42	0.7679	0.0516
18	0.1813	-0.02	43	0.8187	0.0404
19	0.1355	-0.02	44	0.8645	0.0301
20	0.0955	-0.02	45	0.9045	0.021
21	0.0618	-0.0194	46	0.9382	0.0134
22	0.0351	-0.0168	47	0.9649	0.0075
23	0.0157	-0.0122	48	0.9843	0.0033
24	0.0039	-0.0063	49	0.9961	0.0008
25	0	0	50	1	0

Table 1: Wing section co-ordinates in percent chord

3.4 Experimental procedure

The belt velocity was synchronised with the air stream velocity, V = 20 m/s. This corresponded to a dynamic free stream pressure q of 242 Pa and a Reynolds number of $R_e = 2.2 \times 10^5$. The angle of attack was varied from –9° to 37°, in 2° increments. The ground clearance h, which was measured vertically from the trailing edge of the wing to the surface of the moving ground plane (figure 1), was varied from 10 mm (h_0 = 0.06) to 290 mm (h_0 = 1.80). For $h_0 > 1$, where the influence of the ground was expected to be less, the ground clearance was changed in 20 and 40 mm increments. Below $h_0 = 1$, the ground clearance was

changed in 10 mm increments. The data was corrected for tare and interference, while boundary corrections were applied as specified by Barlow *et al.*[15].

4. Results and Discussion

4.1 Lift coefficient, C_L

The C_L data are plotted in figures 3 and 4 as functions of α and h_0 respectively. In figure 3, the increase in α_{L0} is due to the increase in the slope of the lift curve, $\partial C_L/\partial\alpha$, and is similar to the results of Fink and Lastinger[10], and, Serebrisky and Biachuev[11].

The stall angle is identified as that angle where a sudden decrease in lift occurs, and figure 3 shows that the stall angle remains approximately constant as the ground is approached until at about $h_0 = 0.37$, when a further decrease in height causes a significant increase in the stall angle with the stall itself decreasing in severity. It is seen that for $h_0 = 0.06$ there is insufficient data to identify stall.

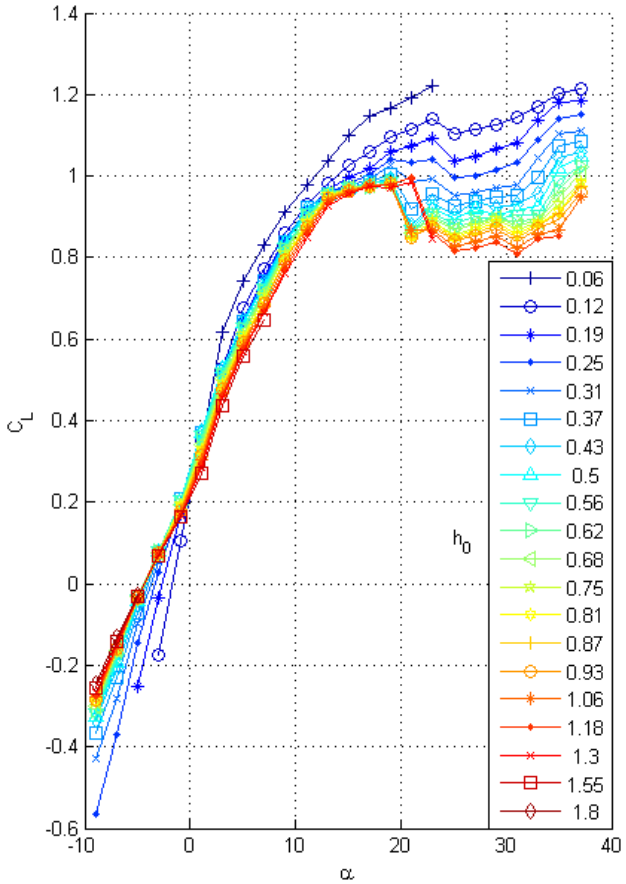

Figure 3: Lift coefficient vs. angle of attack at constant h_0

The change in the slope of the C_L vs. h_0 curve affects the requirement that for the wing to be stable in height, the slope of the C_L vs. h_0 curve should be negative (equation 8). For rearward of the ¼ mac and towards the trailing edge of the wing. For $0.45 < C_L < 0.9$, except for $h_0 = 0.06$, the slopes of the curves are positive and therefore the ACP lies forward of the ¼ mac. Since the slope decreases with a decrease in h_0, this implies that the position of the ACP approaches the ¼ mac with decreasing h_0 positive angles of attack below the stall angle figure 4 indicates a transition of the slope from negative to positive over the region $0.25 < h_0 < 0.5$ (indentified in the brackets). In these regions the wing becomes marginally stable or unstable in height.

At negative angles of attack, there is a decrease in C_L with decreasing h_0. The slope of the curve is positive and the wing is thus unstable in height.

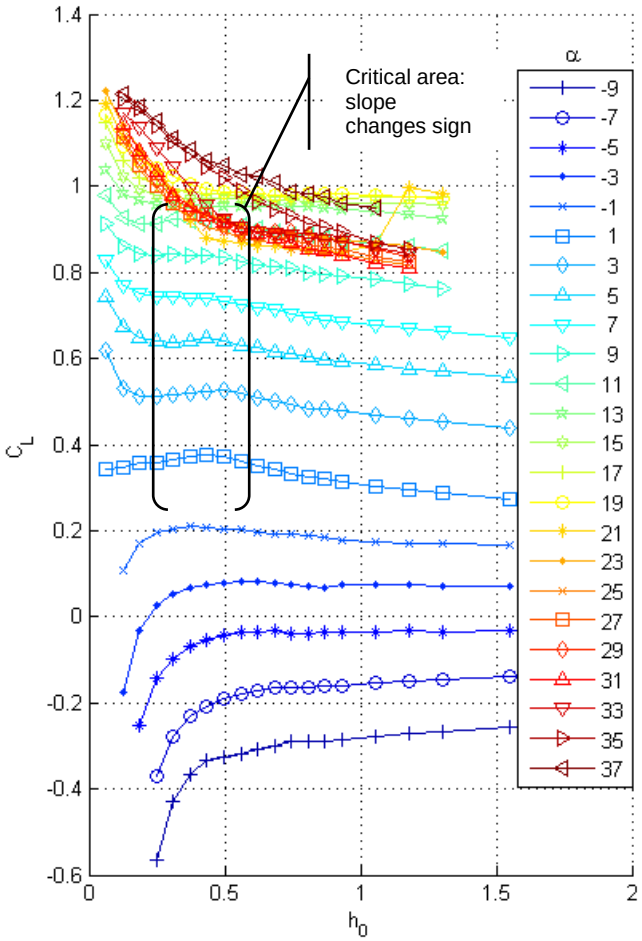

Figure 4: Lift coefficient vs. ground clearance at constant α

4.2 Drag polar

The C_L vs. C_D data are plotted in figure 5 for constant values of h_0. For $0.1 < C_L < 0.4$, C_D increases with decreasing h_0. Over this region, C_D is primarily due to skin friction and form drag, and suggests a net increase in these two effects as the ground is approached. Furthermore, C_{Lmax} increases with decreasing ground clearance. However, C_D at stall is seen to simultaneously increase under these conditions and the efficiency of the wing rapidly deteriorates. Figure 5 also shows that subsequent to stall, L/D decreases for $h_0 > 0.37$, but remains approximately constant for $h_0 < 0.37$.

4.3 Aerodynamic centre in pitch, ACP

The ACP, as determined by equation 5, is most readily observed by considering a plot of the data C_M vs. C_L for constant values of h_0 (figure 6). Each point on a given curve represents a different AoA, and the slope at that point, represents the position of the ACP corresponding to that AoA and value of h_0. Since the moments are given relative to the ¼ mac, a positive slope value indicates the distance is

forward of the ¼ mac, measured along the chord of the wing. A negative value indicates a rearward measurement. The particular region of interest on these curves is that corresponding to $0° < \alpha < \alpha_{stall}$, which approximately corresponds to the lift range $0.2 < C_L < 1.0$ and represents the limits of likely flight cruise angles of attack.

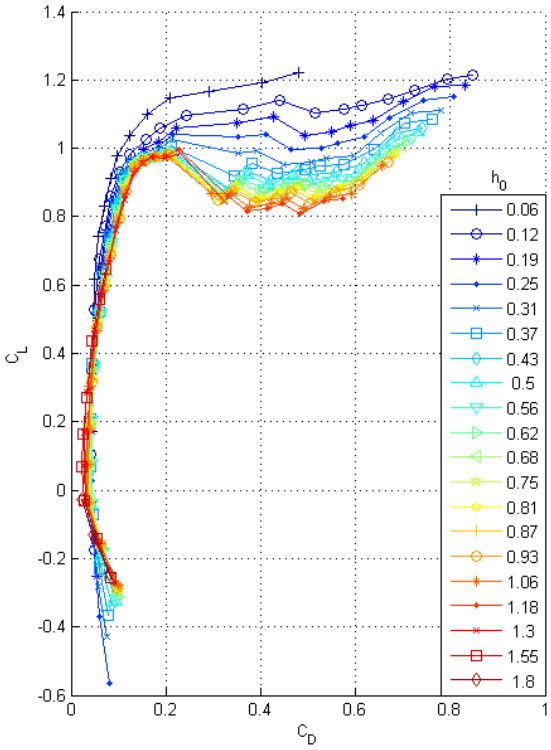

Figure 5: Lift coefficient vs. drag coefficient at constant h_0

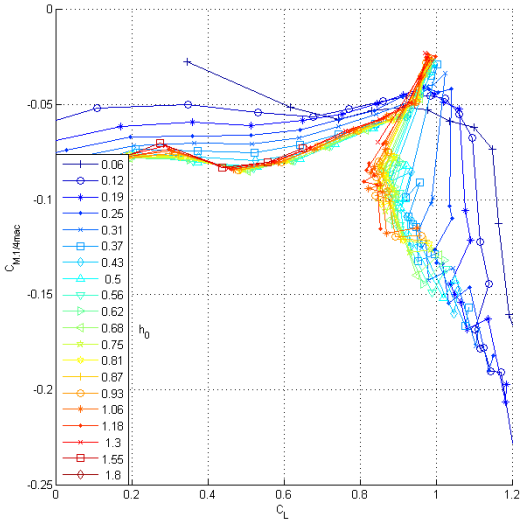

Figure 6: Moment coefficient vs. lift coefficient for constant h_0

For $0.2 < C_L < 0.45$ and $h_0 < 0.43$, the horizontal slope of the curves indicates that C_M is approximately constant with C_L. Thus the position of the ACP is approximately situated at the ¼ mac at these lower ground clearances. For $h_0 > 0.43$, the slopes are negative; therefore the ACP lies.

4.4 Aerodynamic centre in height, ACH

The ACH, as determined by equation 6, is most readily observed by considering a plot of the data C_M vs. C_L for constant values of α (figure 7). Each point on a given curve

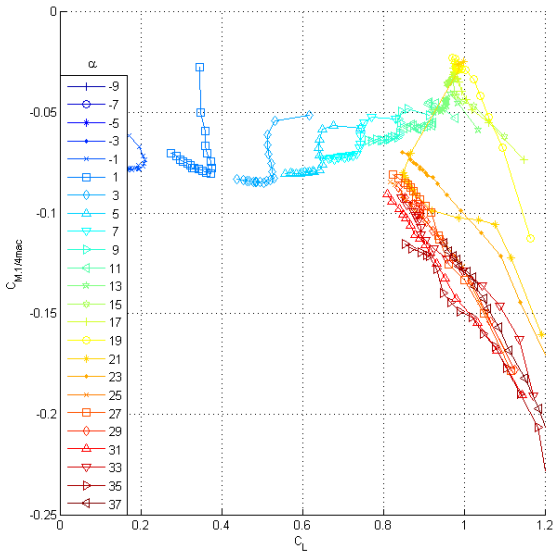

Figure 7: Moment coefficient vs. lift coefficient for constant α

represents a different value of h_0, and the slope at that point, represents the position of the ACH corresponding to that value of h_0 and AoA. Once again, the coordinates are calculated relative to the moment reference axis (¼ mac). The curves of interest are again those corresponding to $0° < \alpha < \alpha_{stall}$ (flight cruise angles), which approximately corresponds to $0.2 < C_L < 1.0$. In figure 7, for $3° < \alpha < 11°$, the S-shaped curves imply that the gradients, and hence X_h, have infinite positive and negative values at certain values of h_0. The shape of the curves are a direct result of the small loss in lift, between $0.19 < h_0 < 0.5$, identified by the critical area in figure 4. For $11° < \alpha < 19°$, the curves display large positive and negative gradients, therefore X_h is expected to move forward and rearward of the ¼ mac.

4.5 Static stability margin, SSM

For stability reasons when in ground effect, it is desirable that the position of both the ACP and ACH remain approximately constant with changing ground clearance and AoA. For the position of the ACH to remain constant with changing h_0, each curve in figure 7 should form a straight line. For the ACH to remain constant with changing α, the slope of each line should be the same. Furthermore, the slope of each curve should be such that the ACH is upstream of the ACP (equation 9).

Figure 8 shows the ACP and ACH vs. h_0 at $\alpha = 3°$. The ACP is seen to remain approximately at the ¼ mac, only moving forward for $h_0 < 0.2$. The ACH is seen to lie predominantly forward of the ACP for $h_0 > 0.7$ (satisfying equation 9). However, at lower ground clearances, the ACH is seen to oscillate between large positive and negative values. This behaviour is again attributed to the critical area identified in figure 4.

Figure 9 shows the ACP and ACH vs.α at h_0 = 0.87. Both curves illustrate a rearward shift of the respective aerodynamic centres with increasing AoA. Furthermore, the relative positions of the two centres predominantly satisfy equation 9.

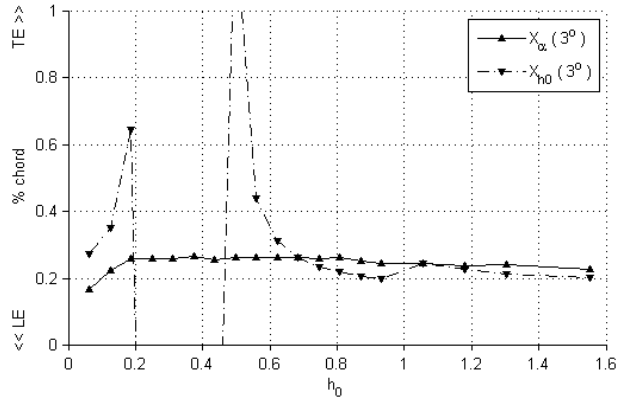

Figure 8: Variation of ACP and ACH with h_0

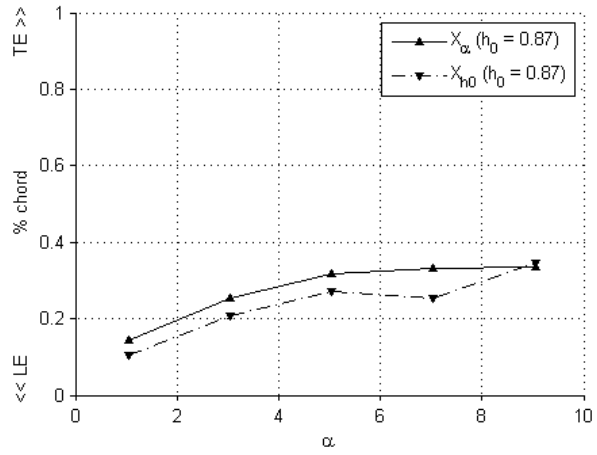

Figure 9: Variation of ACP and ACH with α

For simplicity, figures 8 and 9 only show the ACP and ACH at one AoA and value of h_0 respectively. The figures indicate reasonable performance in consideration of equation 9. However, the trend of the curves was, in general, found to illustrate a rapidly deteriorating SSM over the specified region of interest, with a negative and unstable SSM dominating the flight envelope.

5. Conclusions

The aerodynamic centre in height (ACH) was found to be predominantly downwind of the aerodynamic centre in pitch (ACP). At relative ground clearances, $h_0 < 0.5$, the data indicated significant movement of the ACH. It was concluded that this was a result of a temporary loss in lift as the ground was approached. The data from the analysis indicated that the static stability margin, SSM, was predominantly negative at all ground clearances. Based on these findings, the wing was concluded to be unstable in ground effect. The practical implications of these findings suggest that additional control surfaces would be required to ensure static stability in ground effect.

References

1. *Wieselsberger C*, Wing Resistance Near the Ground, *NACA*, TM-77, 1922.
2. *Rozhdestvensky KV*, Aerodynamics of a Lifting System in Extreme Ground Effect, Springer, Moscow, 2000.
3. *Van Opstal E*, Introduction to WIG technology, *Proceedings of the Euroavia Ground Effect Symposium*, Euroavia, Toulouse, 2001, 13–44.
4. *Rozhdestvensky KV*, Wing-in-ground effect vehicles, *Progress in Aerospace Sciences*, 2006, 42, (3), 211-283.
5. *Kumar PE*, An Experimental Investigation into the Aerodynamic Characteristics of a Wing, With and Without Endplates in Ground Effect, College of Aerodynamics, Cranfield, England, Rept. Aero 201, 1968.
6. *Kumar PE*, Some Stability Problems of Ground Effect Vehicle in Forward Motion, *Aeronautical Quarterly*, 1972, 18, 41–52.
7. *Irodov RD*, Criteria of longitudinal stability of ekranoplan, *Ucheniye Zapiski TSAGI*, 1970, 1 (4), 63-74.
8. *Zhukov VI*, Some matters of longitudinal stability of ekranoplans, *Trudy TSAGI*, 1974.
9. *Staufenbiel RW and Schlichting UJ*, Stability of airplanes in ground effect, *Journal of Aircraft*, 1988, 25, (4), 289-294.
10. *Fink MP and Lastinger JL*, Aerodynamic Characteristics of Low-Aspect-Ratio Wings in Close Proximity to the Ground, *NASA*, TN-926, 1961.
11. *Serebrisky YM and Biachuev SA*, Wind-Tunnel Investigation of the Horizontal Motion of a Wing Near the Ground, *NACA*, TM-1095, 1946.
12. *Gadetski VM*, Investigation of aerodynamic characteristics of the foil with control devices near the ground, *Trudy TSAGI*, Vyp 1256, 1970, 2.
13. *Staufenbiel R and Kleineidam G*, Longitudinal motion of low-flying vehicles in nonlinear flowfields, *Proceedings of the Congress of the International Council of the Aeronautical Sciences*, Munich, 1980, 293–308.
14. *Van Opstal E*, *The Wig Page*, http://www.se-technology.com/wig, January, 2004.
15. *Barlow JB*, *Rae WH and Pope A*, Low-Speed Wind Tunnel Testing, John Wiley and Sons, 3rd ed., New York, 1999.